Lasers Med Sci (2015) 30:1357–1365
DOI 10.1007/s10103-015-1742-5

ORIGINAL ARTICLE

Nanoparticle-loaded macrophage-mediated photothermal therapy: potential for glioma treatment

Steen J. Madsen[1] · Catherine Christie[2,4] · Seok Jin Hong[3,4] · Anthony Trinidad[4] · Qian Peng[5] · Francisco A. Uzal[6] · Henry Hirschberg[1,4]

Received: 24 July 2014 / Accepted: 9 March 2015 / Published online: 21 March 2015

Abstract Gold-based nanoparticles have been used in a number of therapeutic and diagnostic applications. The purpose of this study was to investigate the efficacy of gold–silica nanoshells (AuNS) in photothermal therapy (PTT) of rat gliomas. Rat alveolar macrophages (Ma) were used as nanoparticle delivery vectors. Uptake of AuNS (bare and PEGylated) was investigated in Ma. AuNS were incubated with Ma for 24 h. Phase contrast microscopy was used to visualize the distribution of loaded Ma in three-dimensional glioma spheroids. PTT efficacy was evaluated for both empty (Ma) and AuNS-loaded Ma (Ma^{NS}) in both monolayers and spheroids consisting of C6 rat glioma cells and Ma. Monolayers/spheroids were irradiated for 5 min with light from an 810-nm diode laser at irradiances ranging from 7 to 28 W cm^{-2}. Monolayer survival was evaluated using a 3-(4,5-dimethylthiazol-2-yl)-5-(3-carboxymethoxyphenyl)-2-(4-sulfophenyl)-2H-tetrazolium (MTS) assay while PTT efficacy in spheroids was determined from growth kinetics and live/dead fluorescence microscopy. PTT efficacy was investigated in vivo using a Sprague–Dawley rat glioma model. Five rats received direct intracranial injection of a mixture of 10^4 C6 glioma cells and, 2 days later, an equal number of Ma^{NS}. Three rats received laser treatment (810 nm; 10 min; 1 W) while the remaining two served as controls (no laser treatment). The uptake ratio of bare to PEGylated AuNS by Ma was 4:1. A significant photothermal effect was observed in vitro, albeit at relatively high radiant exposures (2.1–4.2 kJ cm^{-2}). PTT proved effective in vivo in preventing or delaying tumor development in the PTT-treated animals.

Keywords Glioma · Photothermal therapy · Gold–silica nanoshells · Rat macrophages

✉ Steen J. Madsen
steen.madsen@unlv.edu

[1] Department of Health Physics and Diagnostic Sciences, University of Nevada, 4505 South Maryland Pkwy, Las Vegas, NV 89154, USA

[2] Department of Neurosurgery, University of California, Irvine, CA 92612, USA

[3] Department of Otorhinolaryngology–Head and Neck Surgery, Kangbuk Samsung Hospital, Sungkyunkwan University School of Medicine, Seoul, Korea

[4] Beckman Laser Institute and Medical Clinic, University of California, Irvine, CA 92612, USA

[5] Pathology Clinic, Rikshospitalet–Radiumhospitalet HF Medical Center, University of Oslo, Montebello, Oslo N–0310, Norway

[6] School of Veterinary Medicine, University of California, Davis, San Bernardino, CA, USA

Introduction

Primary brain tumors are neoplasms that originate from the parenchymal elements of the brain. There are approximately 17,000 new cases of primary brain tumors diagnosed within the USA every year and an equal number in the EU region [1]. Approximately 40 % of these are of the most malignant variety, glioblastoma multiforme (GBM). Five-year survival rates are dismal (<5 %) [2]. Failure of treatment is usually due to local recurrence at the site of surgical resection indicating that a more aggressive local therapy could be of benefit. Intracavity therapy offers the possibility of applying various treatment modalities (brachytherapy and photodynamic and thermal therapies) aimed at the nests of tumor cells remaining in the resection margin while minimizing damage to normal tissue.

Many human tumors including gliomas contain large numbers of tumor-associated macrophages (TAMs) [3, 4]. In

general, TAMs are derived from peripheral blood monocytes recruited from the local circulation by chemotactic factors or from microglia in the CNS. These innate immune cells can comprise up to 70 % of the cell mass in breast carcinoma and 30–40 % of cells in gliomas [5]. TAMs are found in both vascularized tumor stromal areas and in avascular, hypoxic/necrotic areas, at relatively high cell densities, the latter effect probably owing to their role in angiogenesis and the release of macrophage chemo-attractants such as vascular endothelial growth factor [6]. Macrophage-based vectorization of genes, drugs, or nanoparticles has therefore been suggested for cancer therapy in the brain as a way of targeting nanoparticle delivery and bypassing the blood–brain barrier (BBB) which normally prevents anti-cancer agents from reaching the targeted malignant cells [7, 8]. Cell-based vectorization of therapeutic agents has significant potential for cancer therapy in that it can target and maintain an elevated concentration of therapeutic agents such as nanoparticles at the tumor site and prevent their spread into healthy tissue. The use of such cells is considered of limited risk since macrophages have a relatively short life span and their accumulation occurs naturally in response to tumor development.

A wide variety of gold-based nanoparticles has been investigated for diagnostic and therapeutic applications. Of particular interest are gold–silica nanoshells and gold nanorods since their dimensions and/or compositions can be tailored for optimum absorption of near-infrared (NIR) light which has significant penetration in biological tissues. In the case of gold–silica nanoshells (AuNS), the peak absorption resonance is adjusted by varying the dielectric silica core to gold shell ratio. The ability of gold nanoparticles to convert NIR to heat far exceeds that of conventional dyes, and therefore, they have the potential to be used in hyperthermia applications such as photothermal therapy. The goal of photothermal therapy (PTT) in this context is to induce rapid heating in tumors infiltrated with gold nanoparticles while minimizing thermal diffusion to surrounding normal tissue (Fig. 1). PTT efficacy depends on a number of factors including nanoparticle concentration in the target tissue, laser power density, exposure time, and blood perfusion. In a previous in vitro study, NIR laser-irradiated multicell human glioma spheroids, infiltrated with AuNS-loaded murine monocytes, demonstrated complete growth inhibition in an irradiance-dependent manner [9]. The use of murine monocytes though precludes their use in in vivo rat glioma tumor models of PTT. We have therefore examined the ability of rat alveolar macrophages loaded with AuNS to infiltrate and facilitate PTT of rat glioma cells in vitro, *b*oth as monolayers and as multicell three-dimensional spheroids. In vivo studies were performed to investigate the ability of PTT to inhibit tumor development following intracranial injection of glioma cells followed by injection of Ma^{NS} and NIR laser irradiation.

Materials and methods

Cell lines

Rat alveolar macrophages (NR8383; ATCC# CRL-2192) and C-6 rat glioma cells (ATCC# CCL-107) were obtained from the American Type Culture Collection (Manassas, VA). Both cell lines were maintained in advanced Dulbecco's modified Eagle's medium (DMEM) (Life Technologies, Carlsbad, CA) supplemented with 2 % heat-inactivated fetal bovine serum (FBS), 25 mM HEPES buffer, 100 U/ml penicillin, and 100 μg/ml streptomycin at 37 °C, 5 % CO_2, and 95 % humidity. The adherent glioma cell line was grown in monolayer

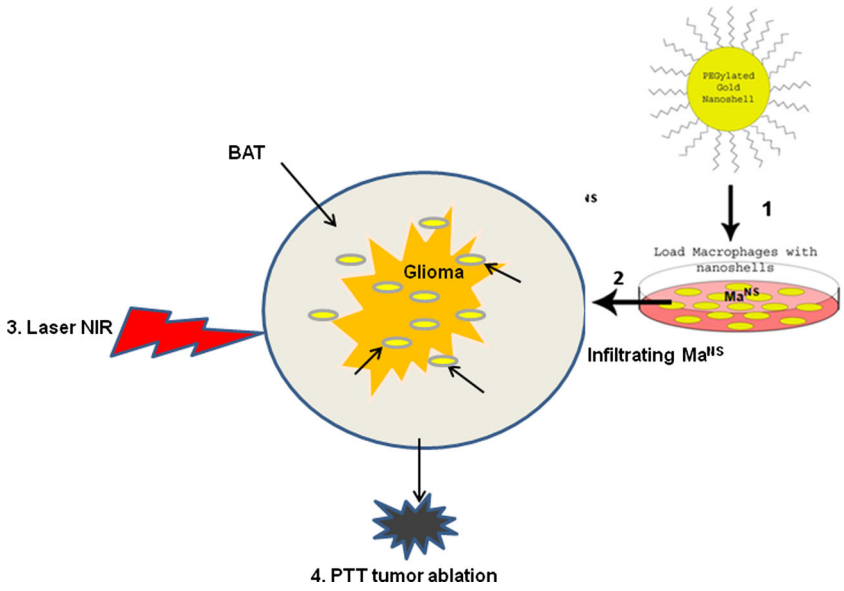

Fig. 1 Overview of PTT via macrophage-mediated delivery of nanoparticles into tumors. Rat alveolar Ma incubated with AuNS for 24 h forming Ma^{NS} (*1*). Ma^{NS} infiltrate tumor and brain adjacent to tumor (BAT) (*2*). Laser irradiation at λ=810 nm (PTT) (*3*). Cell death/tumor ablation (*4*)

whereas the semi-adherent rat macrophage line required scraping during passing.

Experimental animals

Inbred male Sprague–Dawley rats (Charles River, Wilmington, MA) weighing approximately 350 g were used in this study. Animal care and protocols were in accordance with institutional guidelines. Animal holding rooms were maintained at constant temperature and humidity on a 12-h light and dark schedule at an air exchange rate of 18 changes per hour.

Nanoparticles

The gold nanoshells used in this study consisted of a 120-nm silica core with a 12–15-nm gold shell (Nanospectra Biosciences, Inc., Houston, TX). The resultant optical absorption peak was between λ=790 and λ=820 nm for PEGylated particles. The particular batch used in this study had a concentration of 1.41×10^{11} particles/ml with an absorbance peak at 819 nm (optical density of 105). The optical density at the irradiation wavelength (810 nm) was 103. Bare nanoshells (4.29×10^{9} particles/ml) were used in macrophages (Ma) uptake studies. Bare nanoshells have a tendency to aggregate, and therefore, the stock concentration was approximately 33 times lower than the PEGylated AuNS.

Ma–AuNS incubation

Rat alveolar Ma were seeded in 35-mm cell culture dishes at 1×10^{6} Ma in 2 ml of culture medium. The dishes were incubated overnight to allow the cells to settle and adhere to the plastic. Culture medium was exchanged for 100 μl of PEGylated (1.41×10^{11} particles/ml) AuNS colloid in 1.9 ml of culture medium. The Ma were incubated for 24 h at 37 °C, rinsed three times with Hanks' balanced salt solution (HBSS) with calcium chloride and magnesium chloride (Gibco, Carlsbad, CA) to wash away any non-ingested nanoshells. AuNS-loaded Ma were then detached with trypsin and a rubber spatula followed by washing and counting. The concentration of nanoshells in Ma was studied using a UV–vis–NIR spectrophotometer (Varian UV–vis–NIR spectrophotometer Cary 6000i, Varian, USA). Absorbance was measured in cell suspensions over a wavelength range of 600–1100 nm, which covers the broad absorption peak of AuNS. Detailed information can be found in [9].

PTT of monolayer cultures

All light treatment was performed at a culture temperature of 37 °C. For PTT treatment, eight wells in a vertical column in 96-well ultra-low-adhesion round-bottomed plates (Corning Inc., NY) were seeded with either Ma, Ma^{NS}, or C6 + Ma^{NS} at a total density of 5000 cells per well. The plates were centrifuged at 1000*g* for 10 min to force the cells into a small disk at the bottom of the well and incubated for 24 h prior to experimentation. Cells were plated into every fourth column (eight wells) in order to minimize the contribution of light scatter to the non-treated cultures. For PTT, individual wells were irradiated with λ=810-nm CW laser light (Class 3b; Intense, New Brunswick, NJ) at irradiances ranging from 0 to 28 W/cm^2 with a beam diameter of approximately 3 mm. Monolayers in each well were irradiated from the bottom of the plate. The distance between the distal end of the fiber and the bottom surface of the well plate was 0.5 cm. A laser exposure time of 5 min was used. A laser power meter (Field Mate; Coherent, Inc., Santa Clara, CA) was used to measure light intensities at both 810 and 670 nm.

Following laser irradiation, incubation was continued for 48 h, at which point, the culture medium was replaced with fresh clear buffer containing 3-(4,5-dimethylthiazol-2-yl)-5-(3-carboxymethoxyphenyl)-2-(4-sulfophenyl)-2H-tetrazolium (MTS, Promega, Madison, WI) which was used to determine cell viability after PTT treatment. Cells were incubated in MTS reagents for 2 h. The optical density was measured using an ELx800uv Universal Microplate Reader (Bio-Tek Instruments, Inc, Winooski, VT).

Hybrid spheroid generation

Hybrid tumor/Ma spheroids were formed as previously described [9, 10]. Prior to spheroid formation, both Ma^{NS} and Ma were incubated for 1 h in 20 μg ml^{-1} mitomycin C (Sigma-Aldrich Corp., St. Louis, MO) in order to inhibit cell division and their subsequent contribution to spheroid growth. Five thousand C6 tumor cells and a variable number of Ma^{NS} (maximum tumor/Ma^{NS} ratio of 1:1) were investigated. The tumor cell–Ma^{NS} mixture was added to 200-μl culture medium per well of an ultra-low attachment surface 96-well round-bottomed plate (Corning Inc., Corning, NY). The plates were centrifuged at 1000*g* for 10 min. Immediately following centrifugation, the cells formed a disk shape. The plates were maintained at 37 °C in a 5 % CO_2 incubator for 48 h to allow the cell clusters to assume their typical three-dimensional spheroid shape.

PTT of spheroids

Individual spheroids in each well of a 96-well round-bottomed plate were irradiated with 810-nm CW laser light from a laser diode array (Class 3b; Intense, New Brunswick, NJ) at irradiances of 14 or 28 W cm^{-2} with a beam diameter of approximately 3 mm and an irradiation time of 5 min. The irradiation geometry, including the fiber-to-surface distance, was identical to that previously described for the monolayer cultures.

Treatment efficacy was monitored from spheroid growth kinetics and live/dead fluorescence microscopy. Spheroid growth was measured using an ordinary light microscope with a calibrated eyepiece. Fluorescence microscopy was initiated 2 days following treatment. Spheroids were transferred to imaging petri dishes, stained with Hoechst 33342 and ethidium homodimer 1 (Life Technologies, Carlsbad, CA), and imaged using an inverted laser scanning microscope (LSM 410, Carl Zeiss, Jena, Germany). This system allows the differential visualization of cell nuclei using confocal and two-photon microscopy. Blue (live) and red (dead) fluorescence were isolated by using bandpass filters with transmissions of 390–465 nm (blue) and 565–615 nm (red).

PDT of spheroids

Photodynamic therapy (PDT) was used as a control treatment to gauge the efficacy of PTT. C6–Ma^{NS} spheroids were formed as preciously described. Forty-eight hours later, hybrid spheroids were incubated with 1 μg/ml of the photosensitizer $AlPcS_{2a}$ (Frontier Scientific, Inc, Logan, UT) and DMEM for 18 h and washed three times. Irradiation was performed using λ=670-nm light from a CW diode laser (Class 4; Intense, North Brunswick, NJ). The cells were exposed to a radiant exposure of 1.5 J cm^{-2} at an irradiance of 5 mW cm^{-2} through an opaque mask that allowed illumination of one column of eight wells at a time. The distance between the distal end of the fiber and the surface of the well plate was 11.5 cm.

In vivo PTT

Newly implanted C6 glioma cells were used as a proxy to simulate infiltrating cells remaining in the resection margin following surgical removal of bulk tumor. Anesthetized rats (n=5) were fixed in a stereotactic frame. The skin was incised and a 1.0-mm burr hole was made at the following coordinates: 1 mm posterior to the bregma, 2 mm to the right of the midline, and at a depth of 2 mm. The injection device consisted of a 30-G blunt cannula connected through a catheter (Hamilton Co., Reno, NV) to an infusion pump (Harvard Apparatus, Holliston, MA). The cannula was fixed in the electrode holder of the stereotactic frame and then vertically introduced into the brain. A total of 10^4 C6 cells in 10 μl PBS were injected into the brain over a period of 2 min. Following injection, the cannula remained in place for 2 min. Closure was done with bone wax and sutures. Forty-eight hours later, three of the animals were placed in the frame and injected with 10^4 Ma^{NS} as previously described. The injection cannula was then replaced by a 200-μm (dia.) laser fiber inserted 1 mm into the brain through the original burr hole. Following placement of the optical fiber, CW laser irradiation (810 nm) was initiated for a period of 10 min at a total laser power output of 1 W. The fiber was withdrawn and closure was done with bone wax and sutures as before. The two control animals implanted with C6 cells but not subjected to laser irradiation acted as non-treated controls.

Histological preparation

Animals were sacrificed 15 days following implantation and their brains extracted. Brains were fixed by immersion in 10 % buffered (pH 7.2) formalin prior to paraffin embedding. Coronal sections (4 μm thick) were obtained at the point of cell implantation. The sections were stained with hematoxylin and eosin (H&E).

Statistical analysis

Microsoft Excel was used to determine the mean, standard deviation, and standard error. Data were analyzed using one-way ANOVA at the significance level of $p<0.05$ and presented as mean with standard error unless otherwise noted.

Results

Ma endocytosis of bare or PEGylated nanoshells

The phase contrast microscopy images in Fig. 2a, b provide a visual confirmation of AuNS uptake. The internalized NS in Ma are visualized as dark opaque regions in Fig. 2b. These dark areas are absent in the control "empty" Ma (Fig. 2a). As shown in Fig. 2c, rat alveolar Ma demonstrated significant uptake of bare nanoshells; the uptake was approximately four times greater than that of PEGylated nanoshells. However, since the PEGylated nanoshell solution was available at a much higher concentration, it was used in all subsequent experiments. Based on spectrophotometric analyses, 1×10^6 Ma incorporated 30×10^8 PEGylated nanoshells versus 3.5×10^8 bare nanoshells.

In vitro PTT

PTT on Ma^{NS}

The effects of NIR irradiation on 5000 Ma and Ma^{NS} in monolayer culture are shown in Fig. 3a. In both cases, cells were exposed to NIR laser powers of 0, 7, 14, or 28 W cm^{-2} delivered with a beam size of 3 mm. Viability of the Ma^{NS} was reduced to 35 and 12 % of control values at an irradiance of 14 or 28 W cm^{-2} administered over a 5-min period respectively. No significant cytotoxicity was observed for Ma even at irradiances of 28 W cm^{-2} for 5 min.

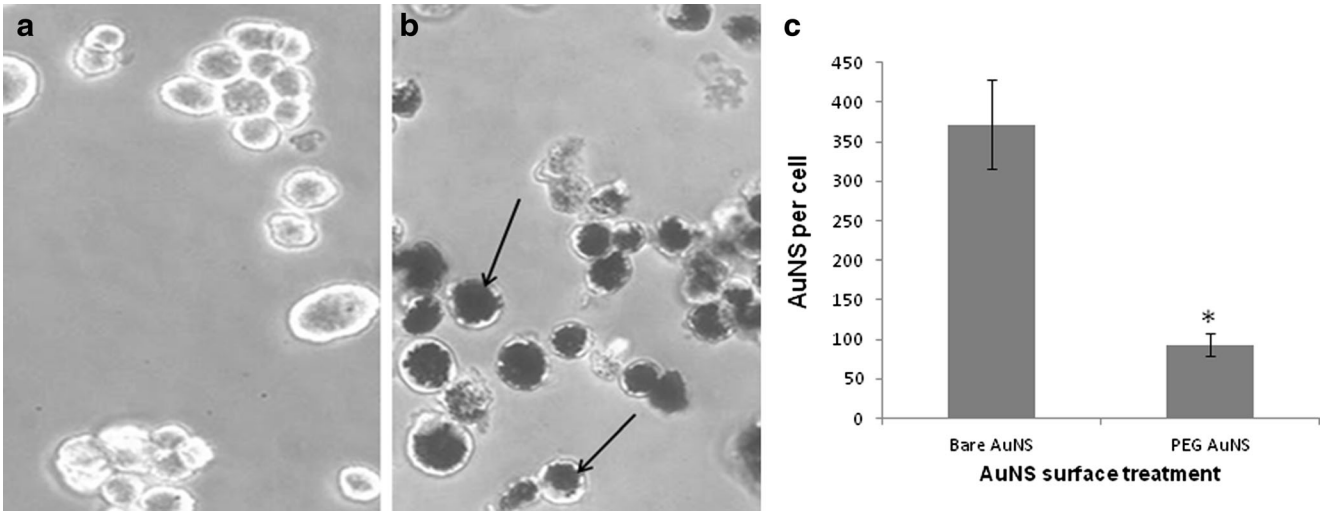

Fig. 2 Phase contrast micrographs (×10 magnification) of non-loaded (**a**) and AuNS-loaded (**b**) rat alveolar macrophages. Macrophages were incubated with AuNS for 24 h. The AuNS appear as *dark*, *opaque regions* in **b** (*arrows*). AuNS uptake by Ma was evaluated from spectrophotometric analysis (**c**). Both PEGylated and bare nanoparticles were examined. Uptake differences between PEG Ma^{NS} and Ma^{NS} were statistically significant ($p<0.05$)

PTT on combined C6–Ma^{NS} monolayers and hybrid spheroids

The effects of Ma^{NS}-mediated PTT in a C6 glioma cell line are illustrated in Fig. 3b. A significant decline in cell viability with increasing irradiance was observed: viability was reduced to approximately 15 % of controls following an irradiance of 28 W cm^{-2} (2:1 C6–Ma ratio). Not surprisingly, a substantial increase in PTT efficacy could be realized by doubling the number of Ma^{NS} (1:1 ratio). In this case, effects were observed even at the lowest irradiance (7 W cm^{-2}) which resulted in 70 % survival (compared to 100 % survival for the 2:1 case). The effect of the higher Ma^{NS} concentration was especially pronounced at the highest irradiance where cell survival was reduced to approximately 5 % of controls.

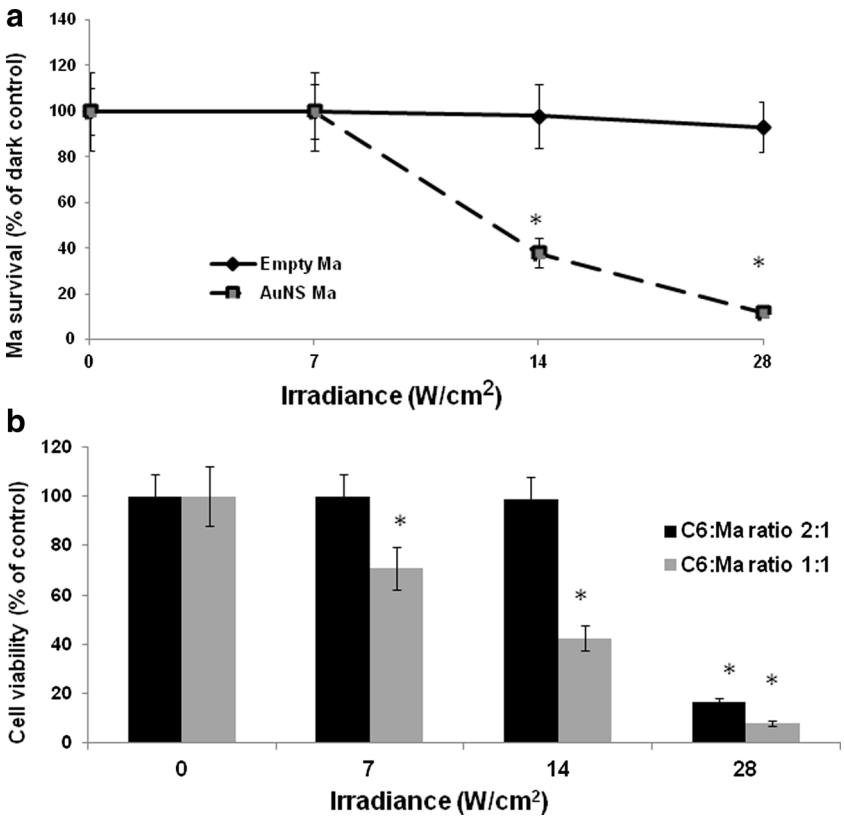

Fig. 3 **a** Effects of NIR irradiation on Ma and Ma^{NS} in monolayer culture. Five thousand Ma or Ma^{NS} were exposed to NIR laser irradiances of 0, 7, 14, or 28 W cm^{-2} delivered with a beam size of 3 mm for 5 min. Cell viability was determined by MTS assay. The results are shown as % of non-irradiated controls. Each data point corresponds to the mean of three trials, and *error bars* denote standard errors. **b** Ma^{NS}-mediated PTT in a C6 rat glioma cell line. Ma^{NS} and C6 cells were exposed to 810-nm laser light at irradiances of 0, 7, 14, or 28 W cm^{-2} for 5 min. Two different C6/Ma ratios were investigated, and the PTT effect was evaluated using an MTS assay. *Asterisks* denote statistical significance ($p<0.05$)

Hybrid C6/Ma spheroids were formed as described in the "Materials and methods" section. The phase contrast micrograph (Fig. 4a) composed of C6 and Ma^{NS} at a ratio of 4:1 illustrates the even distribution of Ma^{NS} throughout the spheroid. C6/Ma^{NS} hybrid spheroids showed a similar sensitivity to PTT as was seen in the monolayer cultures. This is clearly illustrated in two-photon live/dead microscopy as shown in Fig. 4b. At an irradiance of 14 W cm^{-2}, only a small fraction of the cells (mostly located at the periphery of the spheroid) were dead (red). The vast majority of glioma cells in the center were found to be viable (blue). In contrast, most of the cells were dead following NIR exposure to 28 W cm^{-2} for 5 min. Figure 4c shows the growth kinetics of hybrid spheroids following PTT. A significant decrease in spheroid volume after 20 days in culture was observed following 5 min of λ=810-nm laser irradiation (28 W cm^{-2}) at all the C6/Ma^{NS} ratios examined (2:1–8:1). The effect was especially pronounced in the spheroids with the largest number of Ma^{NS} where no growth was observed throughout the observation period.

Comparison of PDT and PTT toxicity

As illustrated in Fig. 4d, Ma/C6 hybrid spheroids subjected to PDT (5 mW cm^{-2}; 5 min) showed similar survival compared to PTT-treated (14 W cm^{-2}; 5 min) Ma^{NS}/C6 spheroids. Based on these results, PDT is a more efficient treatment modality since the observed toxicity was accomplished with a total radiant exposure of 1.5 J cm^{-2} which is 2800 times lower than that used in the PTT treatment (4200 J cm^{-2}).

In vivo PTT

In order to determine if the PTT results obtained in vitro could be reproduced in vivo, animals were placed in a stereotactic frame and injected with 10^4 C6 cells directly into the brain. Forty-eight hours later, 10^4 Ma^{NS} were injected into the same area used for C6 implantation. Laser irradiation (810 nm; 1 W; 10 min) was initiated shortly following Ma^{NS} injection. Control animals received C6 cells and no NIR laser treatment. Thirteen days following PTT treatment, animals were

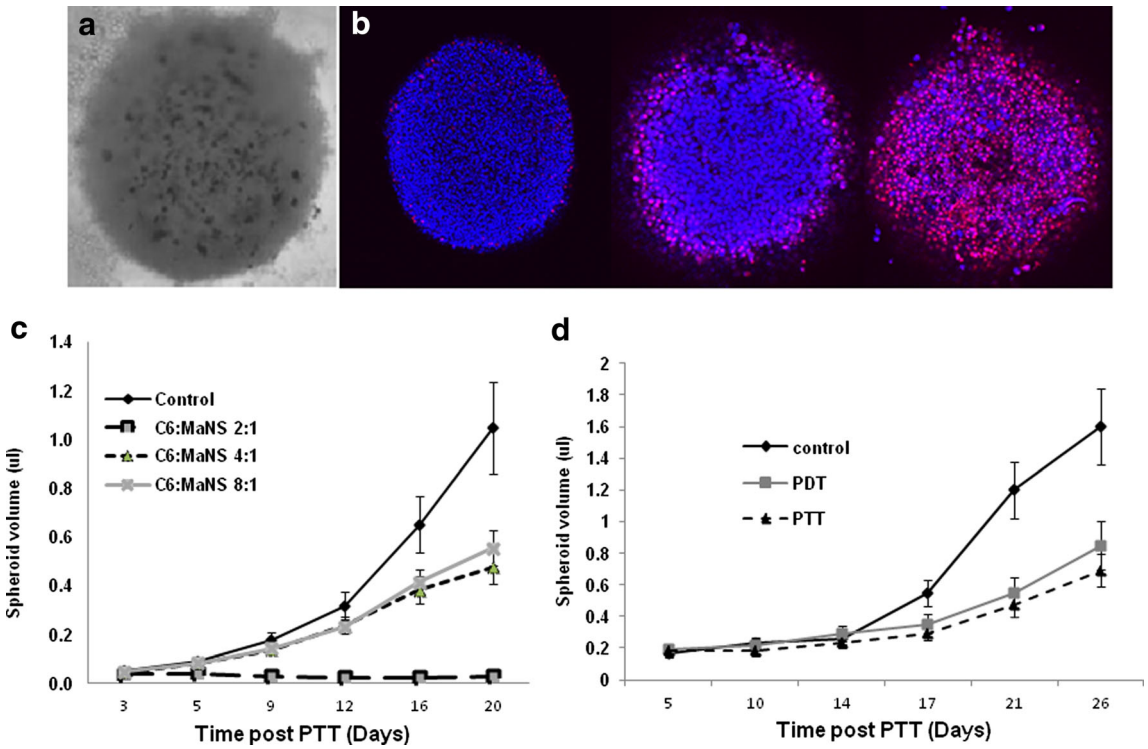

Fig. 4 **a** Phase contrast micrograph of C6/Ma^{NS} spheroid (700-μm dia.) Ma^{NS} appear as dark aggregates and are evenly distributed throughout the spheroid. **b** Live/dead assay of PTT-treated C6/Ma^{NS} spheroids. Two-photon micrographs were made at planes 100 μm into the spheroids with simultaneous excitation of two dyes (*blue*—live; *red*—dead). Spheroids were irradiated with 810-nm laser light for 5 min at irradiances of 0, 14, or 28 W cm^{-2}. Images were acquired 2 days post-PTT. In all cases, a 600× 600-μm field of view was used. **c** Hybrid spheroid survival as a function of Ma^{NS} concentration. Five thousand C6 and a variable number of Ma^{NS} (C6 to Ma^{NS} ratios of 2:1, 4:1, and 8:1) were subjected to 810-nm laser irradiation for 5 min at an irradiance of 28 W cm^{-2}. Spheroid growth was followed for 20 days post-irradiation. Control corresponds to hybrid spheroids (2:1 ratio) that received no irradiation. Each data point corresponds to the mean of three trials, and *error bars* denote standard errors. **d** Comparison of radiant exposure for PDT (λ=670 nm; 5 mW cm^{-2}; 5 min) and PTT (λ=810 nm; 14 W cm^{-2}; 5 min) toxicity in hybrid spheroids. Spheroids in the PDT study were incubated in 1 μg ml^{-1} $AlPcS_{2a}$ for 18 h prior to irradiation. Each data point represents the mean of three experiments. *Error bars* denote standard errors

euthanized, their brains removed and sectioned into halves at the point of cell inoculation, and H&E-stained sections prepared. Figure 5a, b shows low-power macro photographs from typical untreated and PTT-treated brains, respectively. As can be seen from Fig. 5a, a large cell dense tumor, extending from the cortex to the ventricular system, developed in the untreated animal. In contrast, a small tumor remnant can be seen in one of the PTT-treated animals (arrow; Fig. 5b). In addition, clear tissue damage is seen surrounding the treated area. The extent of the tumor in the untreated animal is clearly evident in the H&E section (Fig. 5c) while the tumor remnant in the treated animal is indicated by the arrow in Fig. 5d. In the other 2 PTT-treated animals (Fig. 5e, f), no evidence of tumor development was observed in the histological sections, but some tissue changes were apparent as indicated by the arrows.

Discussion

Localized delivery of nanoparticles forms the basis for a number of investigative therapeutic approaches including selective tumor heating via PTT. In the present study, exogenous rat Ma were used as delivery vehicles for gold-based nanoparticles. Since Ma are efficient scavengers of pathogens, it was hardly surprising that nanoshells were readily phagocytosed even after PEGylation. The explanation for this observation is uncertain since the biophysical mechanisms of phagocytosis have not been elucidated. The few studies that have been published have focused primarily on polymer micro-particles since these are similar in size to biologic pathogens [11]. It is well established that size, shape, and surface chemistry influence phagocytosis [12, 13]. For example, smaller particles are more readily phagocytized than larger ones as are particles with shapes similar to pathogens such as bacteria. The effects of surface chemistry on phagocytosis have been studied extensively. It is well known that the addition of a polyethylene glycol (PEG) coating impairs phagocytosis by delaying opsonization or adsorption of proteins which enhances phagocytosis [14]. It is precisely for this reason that PEGylated nanoparticles are used for in vivo applications; reduced Ma uptake increases biodistribution times and nanoparticle concentrations in target tissues. The data in Fig. 2 show that pegylation of AuNS decreased uptake by Ma by a factor of approximately 4. Since PEGylation prevents aggregation, higher concentrations of nanoparticles in solution are possible. The concentration of the PEGylated AuNS solution used in these studies was approximately 33 times higher compared to that of the bare AuNS solution, and thus, the total amount of PEGylated AuNS taken up by the Ma was approximately eight times higher than that of the bare AuNS. The increased loading of PEGylated AuNS into Ma makes them ideally suited for PTT applications, and they were therefore used in all studies.

Collectively, the in vitro studies (Figs. 3 and 4) show that a sufficient number of AuNS can be delivered via Ma to

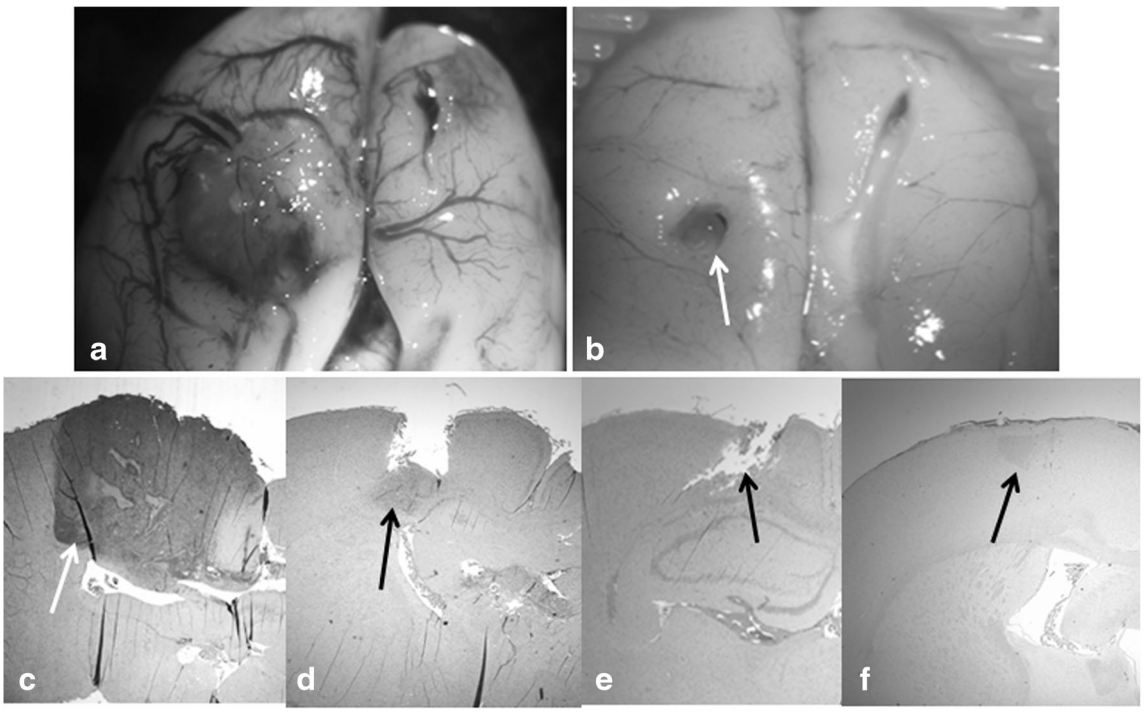

Fig. 5 PTT of C6 rat glioma cells and Ma^{NS} in vivo. Laser-treated animals were subjected to 1 W of 810-nm light for 10 min. Sections were obtained 13 days post-PTT. The light macro image (**a**) and the H&E section (**c**) show significant tumor development in the non-treated control animal. There is a small local tissue defect in the treatment area (**b**), as well as a tumor recurrence below the treatment area in the PTT-treated animal (*arrow*; **d**). The two other PTT-treated animals showed no sign of tumor but developed changes in the treated area (*arrows*; **e**, **f**)

produce a significant PTT effect, albeit at relatively high radiant exposures. For example, significant PTT effects in C6 monolayers and spheroids were only observed at radiant exposures of 2.1 (Fig. 3) and 4.2 kJ cm^{-2} (Fig. 4), respectively. Furthermore, the results in Fig. 3 show that PTT is relatively inefficient compared to PDT. For example, PTT required radiant exposures 2800 times higher than those used in PDT for similar growth inhibition. Nevertheless, PTT does offer some advantages that may make it appealing from a clinical perspective. Unlike PDT, PTT does not require oxygen for its effects, and therefore, it may be useful in treatments of highly hypoxic tumors. Additionally, since longer wavelengths are used in PTT, light penetration in tissues is deeper compared to PDT. For example, penetration depths in normal adult brain at 670 and 810 nm are approximately 4.0 and 6.0 mm, respectively [15].

The PTT results are in qualitative agreement with those of Bernardi et al. [16] who demonstrated that AuNS bioconjugated to two different antibodies selectively killed tumor cells overexpressing the targeted biomarkers when exposed to NIR laser irradiation of 80 W cm^{-2} for 2 min, corresponding to a radiant exposure of 9.6 kJ cm^{-2}. The results also illustrate the dependence of PTT efficacy on AuNS concentration: increasing the number of nanoshells results in a dramatic reduction in both cell viability (Fig. 3b) and spheroid growth (Fig. 4a). This underscores the importance of achieving an adequate concentration of AuNS for effective PTT.

Based on the in vitro PTT results, studies were performed to determine PTT efficacy in vivo. As shown in Fig. 5, only a small tumor remnant was observed in one of the treated animals while the other two displayed no tumor development. Taken together, these results suggest that PTT may be a valid approach for the eradication of tumor cells remaining in the resection margin following cytoreductive surgery. The lack of tumor development in the PTT-treated animals is in all probability due to the therapeutic hyperthermia induced by NIR irradiation and the presence of Ma^{NS}. An alternate explanation for the results shown in Fig. 5 might be that the presence of the Ma^{Ns} alone could inhibit tumor growth. Although a control group consisting of non-irradiated Ma^{NS}-injected animals was not included, this alternative explanation seems unlikely. Previous in vitro experiments in both monolayers and spheroids failed to demonstrate differences in growth kinetics between tumor cell–Ma^{NS} (or tumor cell–Ma) mixtures compared to tumor cells only [9, 17]. Ma have therefore not been observed to have an inhibitory effect on tumor cells/tumors, quite the contrary. Patients with extensive Ma infiltration into tumors have a very poor prognosis, suggesting that Ma stimulate tumor growth [18]. Both experimental and clinical studies have shown that the tumor microenvironment shifts Ma and other immune cells to perform functions related to the tumor's needs (oncotraining). These functions are related to chronic inflammation and tissue remodeling and include increased proliferation and survival, increased angiogenesis and vessel permeability, and self-renewal properties that together promote tumor growth and metastasis [19, 20].

As was observed in vitro, high energy levels (0.6 kJ) were required to achieve significant cell kill in vivo. This is in good agreement with the results of Schwartz et al. [21] who investigated the efficacy of AuNS PTT in an orthotopic model consisting of canine transmissible venereal tumor in the canine brain. NIR laser light delivered via an intratumoral optical fiber over 3 min at 3.5 W (0.63 kJ) resulted in substantial thermal ablation of the tumor. Due to the high incident laser power, a water-cooled applicator was used to prevent charring of tissue proximal to the fiber.

The clinical implications of the in vivo PTT study are somewhat uncertain due to the use of a highly idealized model consisting of high concentrations of Ma injected directly into the brain. It is unclear whether such high concentrations are required in order to eradicate infiltrating glioma cells in the brain adjacent to tumor (BAT) region. An additional complicating factor is the presence of the BBB which was circumvented in this study. Recent work by Madsen et al. [22] has shown that exogenously loaded Ma are unable to traverse the BBB in normal rat brain, suggesting that elimination of infiltrating glioma cells requires targeted opening of the BBB prior to Ma administration. This could be accomplished using a variety of targeted approaches including ultrasound, PDT, or photochemical internalization [23]. Since AuNS-mediated PTT is unlikely to be used as a first-line therapy for malignant gliomas, the power levels required are likely to be lower than those needed for bulk tumor ablation. The role of PTT will likely be limited to the eradication of glioma cells remaining in the resection margin and BAT following surgical resection. This could be accomplished using indwelling balloon applicators that, in addition to stabilizing the resection cavity, would ensure a uniform light irradiation field while avoiding the complications associated with tissue charring [24].

Acknowledgments The authors are grateful for support from the Norwegian Radium Hospital Research Foundation. Portions of this work were made possible through access to the LAMMP Program NIBIB P41EB015890 and the Chao Cancer Center Optical Biology Shared Resource at UCI. Steen Madsen was supported, in part, by the Tony and Renee Marlon Charitable Foundation.

Conflict of interest The authors declare that they have no conflict of interest.

Ethical standards All animal studies were approved by the Institutional Animal Care and Use Committee at the University of California, Irvine, and have therefore been performed in accordance with the ethical standards laid down in the 1964 Declaration of Helsinki and its later amendments. The manuscript does not contain clinical studies or patient data.

References

1. Ostrom QT, Gittleman H, Farah P, Ondracek A, Chen Y, Wolinsky Y, Stroup NE, Kruchko C, Barnholtz-Sloan JS (2013) CBTRUS statistical report: primary brain and central nervous system tumors diagnosed in the United States 2006-2010. Neuro Oncol 15(sup 2): ii1–ii56
2. Ahmed R, Oborski MJ, Hwang M, Lieberman FS, Mountz JM (2014) Malignant gliomas: current perspectives in diagnosis, treatment, and early response assessment using advanced quantitative imaging methods. Cancer Manag Res 6:149–170
3. Kushchayev SV, Kushchayeva YS, Wiener PC, Scheck AC, Badie B, Preul MC (2012) Monocyte-derived cells of the brain and malignant gliomas; the double face of Janus. World Neurosurg. doi:10.1016/j.wneu.2012.11.059
4. Badie B, Schartner JM (2000) Flow cytometric characterization of tumor-assisted macrophages in experimental gliomas. Neurosurgery 46:957–962
5. Leek RD, Landers RJ, Harris AL, Lewis CE (1999) Necrosis correlates with high vascular density and focal macrophage infiltration in invasive carcinoma of the breast. Br J Cancer 79:991–995
6. Leek RD, Hunt NC, Landers RJ, Lewis CE, Royds JA, Harris AL (2000) Macrophage infiltration is associated with VEGF and EGFR expression in breast cancer. J Pathol 190:430–436
7. Hirschberg H, Baek S-K, Kwon YJ, Sun C-H, Madsen SJ (2010) Bypassing the blood brain barrier: delivery of therapeutic agents by macrophages. Proc SPIE 7548:75483Z-1-5
8. Madsen SJ, Baek S-K, Makkouk AR, Krasieva T, Hirschberg H (2012) Macrophages as cell-based delivery systems for nanoshells in photothermal therapy. Ann Biomed Eng 40:507–515
9. Baek S-K, Makkouk AR, Krasieva T, Sun C-H, Madsen SJ, Hirschberg H (2011) Photothermal treatment of glioma: an in vitro study of macrophage-mediated delivery of gold nanoshells. J Neurooncol 104:439–448
10. Ivascu A, Kubbies M (2006) Rapid generation of single-tumor spheroids for high-throughput cell function and toxicity analysis. J Biomol Screen 11:922–932
11. Champion JA, Mitragotri S (2006) Role of target geometry in phagocytosis. Proc Natl Acad Sci U S A 103:4930–4934
12. Ahsan FL, Rivas IP, Khan MA, Suarez AI (2002) Targeting to macrophages: role of physicochemical properties of particulate carriers—liposomes and microspheres—on the phagocytosis by macrophages. J Control Release 79:29–40
13. Beningo KA, Wang YL (2002) Fc-receptor-mediated phagocytosis is regulated by mechanical properties of the target. J Cell Sci 115: 849–856
14. Owens DE III, Peppas NA (2006) Opsonization, biodistribution, and pharmacokinetics of polymeric nanoparticles. Int J Pharm 307:93–102
15. Madsen SJ, Wilson BC (2013) Optical properties of brain tissue. In: Madsen SJ (ed) Optical methods and instrumentation in brain imaging and therapy, 1st edn. Springer, New York, pp 1–22
16. Bernardi RJ, Lowery AR, Thompson PA, Blaney SM, West JL (2008) Immunonanoshells for targeted photothermal ablation in medulloblastoma and glioma: an in vitro evaluation using human cell lines. J Neurooncol 86:165–172
17. Trinidad A, Hong SJ, Madsen SJ, Hirschberg H (2014) Combined concurrent photodynamic and gold nanoshell loaded macrophage-mediated photothermal therapies: an in vitro study on squamous cell head and neck carcinoma. Lasers Surg Med 46:310–318
18. Becker M, Muller CB, De Bastiani MA, Klamt F (2013) The prognostic impact of tumor-associated macrophages and intra-tumoral apoptosis in non-small cell lung cancer. Histol Histopathol 29:21–31
19. Chimal-Ramirez GK, Espinoza-Sanchez NA, Fuentes-Panana EM (2013) Protumor activities of the immune response: insights in the mechanisms of immunological shift, oncotraining and oncopromotion. J Oncol. doi:10.1155/2013/835956
20. Partecke LI, Gunther C, Hagemann S, Jacobi C, Merkel M, Sendler M, van Rooijen N, Kading A, Nguyen Trung D, Lorenz E, Diedrich S, Weiss FU, Heidecke CD, von Bernstorff W (2013) Induction of M2-macrophages by tumor cells and tumor growth promotion by M2-macrophages: a quid pro quo in pancreatic cancer. Pancreatology 13:508–516
21. Schwartz JA, Shetty AM, Price RE, Stafford RJ, Wang JC, Uthamanthil RK, Pham K, McNichols RJ, Coleman CL, Payne JD (2009) Feasibility study of particle-assisted laser ablation of brain tumors in orthotopic canine model. Cancer Res 69:1659–1667
22. Madsen SJ, Gach HM, Hong SJ, Uzal FA, Peng Q, Hirschberg H (2013) Increased nanoparticle-loaded exogenous macrophage migration into the brain following PDT-induced blood-brain barrier disruption. Lasers Surg Med 45:524–532
23. Madsen SJ, Hirschberg H (2010) Site-specific opening of the blood-brain barrier. J Biophoton 3:356–367
24. Madsen SJ, Sun C-H, Tromberg BJ, Hirschberg H (2001) Development of a novel indwelling balloon applicator for optimizing light delivery in photodynamic therapy. Lasers Surg Med 29: 406–412